

Enhancement of the second harmonic generation from monolayer WS_2 coupled with a silica microsphere

Xiao-Zhuo Qi(祁晓卓) and Xi-Feng Ren(任希锋)

Citation: Chin. Phys. B, 2022, 31 (**10**): 104203. DOI: 10.1088/1674-1056/ac6868
Journal homepage: http://cpb.iphy.ac.cn; http://iopscience.iop.org/cpb

What follows is a list of articles you may be interested in

Electrically pumped metallic and plasmonic nanolasers

Martin T Hill

Chin. Phys. B, 2018, 27 (**11**): 114210. DOI: 10.1088/1674-1056/27/11/114210

Detection performance improvement of photon counting chirped amplitude modulation lidar with response probability correction

Yi-Fei Sun(孙怿飞), Zi-Jing Zhang(张子静), Li-Yuan Zhao(赵丽媛), Wei-Min Sun(孙伟民), Yuan Zhao(赵远)

Chin. Phys. B, 2018, 27 (**9**): 094213. DOI: 10.1088/1674-1056/27/9/094213

All polymer asymmetric Mach-Zehnder interferometer waveguide sensor by imprinting bonding and laser polishing

Yu Liu(刘豫), Yue Sun(孙月), Yun-Ji Yi(衣云骥), Liang Tian(田亮), Yue Cao(曹悦), Chang-Ming Chen(陈长鸣), Xiao-Qiang Sun(孙小强), Da-Ming Zhang(张大明)

Chin. Phys. B, 2017, 26 (**12**): 124215. DOI: 10.1088/1674-1056/26/12/124215

Tunable optical filter using second-order micro-ring resonator

Lin Deng(邓林), Dezhao Li(李德钊), Zilong Liu(刘子龙), Yinghao Meng(孟英昊), Xiaonan Guo(郭小男), Yonghui Tian(田永辉)

Chin. Phys. B, 2017, 26 (**2**): 024209. DOI: 10.1088/1674-1056/26/2/024209

High-speed and broad optical bandwidth silicon modulator

Xu Hao, Li Xian-Yao, Xiao Xi, Li Zhi-Yong, Yu Yu-De, Yu Jin-Zhong

Chin. Phys. B, 2013, 22 (**11**): 114212. DOI: 10.1088/1674-1056/22/11/114212

Enhancement of the second harmonic generation from monolayer WS_2 coupled with a silica microsphere

Xiao-Zhuo Qi(祁晓卓)[1,2] and Xi-Feng Ren(任希锋)[1,2,†]

[1] *CAS Key Laboratory of Quantum Information, University of Science and Technology of China, Hefei* 230026, *China*
[2] *CAS Synergetic Innovation Center of Quantum Information and Quantum Physics, University of Science and Technology of China, Hefei* 230026, *China*

(Received 1 March 2022; revised manuscript received 11 April 2022; accepted manuscript online 20 April 2022)

Monolayer transition metal dichalcogenides (TMDs) are widely used for integrated optical and photoelectric devices. Owing to their broken inversion symmetry, monolayer TMDs have a large second-order optical nonlinearity. However, the optical second-order nonlinear conversion efficiency of monolayer TMDs is still limited by the interaction length. In this work, we theoretically study the second harmonic generation (SHG) from monolayer tungsten sulfide (WS_2) enhanced by a silica microsphere cavity. By tuning the position, size, and crystal orientation of the material, second-order nonlinear coupling can occur between the fundamental pump mode and different second harmonic cavity modes, and we obtain an optimal SHG conversion efficiency with orders of magnitude enhancement. Our work demonstrates that the microsphere cavity can significantly enhance SHG from monolayer 2D materials under flexible conditions.

Keywords: integrated optics, frequency conversion

PACS: 42.82.–m, 42.65.Ky **DOI:** 10.1088/1674-1056/ac6868

1. Introduction

Transition metal dichalcogenides (TMDs) are widely used as building blocks for various optical systems due to their significant optical properties.[1] Some kinds of TMDs, such as tungsten sulfide (WS_2),[2] molybdenum sulfide (MoS_2),[3,4] and tungsten selenide (WSe_2),[5] have a large second harmonic generation (SHG) response due to the symmetry breaking of the crystal structure.[6,7] An odd-layer 2H phase TMD can generate a strong second harmonic,[8–10] and the intensity of the SHG signal decreases as the number of layers increases.[6] The SHG from monolayer TMD is not limited by momentum matching because of the much smaller thickness of the monolayer TMD than the pump and harmonic wavelengths.[6,11] However, the thickness becomes a constraint for nonlinear conversion efficiency because of limited interaction length.[11]

Furthermore, coupling TMDs with micro/nanostructures can enhance SHG conversion efficiency. In this way, the evanescent field confined by the micro/nanostructure can directly interact with the material. As an effective method, two-dimensional materials are reported to be coupled with various micro/nanostructures, such as waveguides,[12,13] fibers,[14–16] and microcavities.[1,17,18] In addition, monolayer TMDs can also be fabricated as microscale heterojunctions.[19] In particular, two-dimensional materials coupled with cavity structures can increase the interaction with the electromagnetic field, which can greatly enhance the photoluminescence,[20,21] Raman signal,[22] and SHG.[18] There are a variety of cavity structures that have been used to enhance the coupling strength between the two-dimensional material and the light field, including surface plasmon structures,[21–26] microdisks,[20] microspheres,[17,18,27] photonic crystals,[28,29] metasurfaces,[30,31] and photonic bound states in the continuum.[32] Within these structures, the microsphere cavity has the advantages of a high quality factor and easy fabrication.[17] A research group reported the enhancement of SHG from WS_2 by placing microspheres on monolayer WS_2.[18] However, the SHG conversion efficiency is still low, and particularly the SHG conversion efficiency simultaneously enhanced by microsphere cavity has not been studied in theory.

In this work, we theoretically calculate the SHG conversion efficiency of monolayer WS_2 deposited on the surface of a silica microsphere. We study the cases in which the pump and SHG signals both resonate with the cavity modes in the SHG process. The wavelengths of the pump mode are around 1550 nm and the wavelengths of the SH mode are around 775 nm. Considering the cavity mode symmetry, we study the second-order nonlinear coupling between the fundamental pump mode and the different second harmonic (SH) modes. Monolayer WS_2 can be deposited with different positions, sizes, and crystal orientations on the microsphere, which enables flexible mode to match with odd/even order or different polarization directions. In our simulation, we theoretically obtain an optimized SHG conversion efficiency of 3.35% with 1 mW pump power under a typical quality factor (1×10^6). This result is three orders of magnitude higher than the SHG conversion efficiency of monolayer WS_2 currently reported.[33]

[†]Corresponding author. E-mail: renxf@ustc.edu.cn

© 2022 Chinese Physical Society and IOP Publishing Ltd

2. Model

In our work, monolayer WS_2 is deposited on the surface of a silica microsphere, as shown in Fig. 1(a). The plane of the blue dashed circle is the equatorial plane of the microsphere cavity. The angle θ represents the position of WS_2 relative to the equatorial plane. A coordinate system is established on the surface of the microsphere, where the x axis is in the latitude direction, the y axis is in the longitude direction and the z axis is in the normal direction of the microsphere surface. The length of the material in the x direction is l, and the length in the y direction is w. The monolayer WS_2 studied in this work belongs to the point group of D_{3h}, and the schematic is shown in Fig. 1(b). We set the angle between the b axis of the crystal orientations and the y axis of the surface coordinates as Ω. The thickness of the material is approximately 0.65 nm.[11] The finite element analysis is performed to analyze the coupling strength between the material and the microsphere. Because of the rotational symmetry of the microsphere cavity mode,[34] we use a 2D rotational symmetry model to simplify the simulation model. In the simulation, it is assumed that the material position does not affect the cavity mode because the thickness of the material is three orders of magnitude smaller than the wavelength.

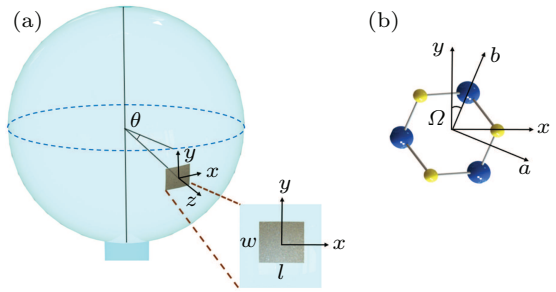


Fig. 1. (a) Schematic of the system. The plane of the blue dashed circle is the equatorial plane. The inset is a schematic of the material with the in-plane coordinates. (b) Demonstration of the angle (Ω) between the crystal orientations (a,b) and the coordinates (x,y).

3. Simulation and results

To obtain the SHG conversion efficiency, we first calculate the nonlinear coupling strength between the pump mode and SH mode[35] when the pump mode and SH mode are double resonances. The electric field of the cavity mode is denoted as $\boldsymbol{E}_j(\boldsymbol{r},t) = a_j\boldsymbol{u}_j(\boldsymbol{r})\,\mathrm{e}^{\mathrm{i}\omega_j t} + a_j^{\dagger}\boldsymbol{u}_j^{*}(\boldsymbol{r})\,\mathrm{e}^{-\mathrm{i}\omega_j t}$, where $j = 1, 2$ represents the pump mode and the SH mode, respectively; $a_j^{\dagger}$ and a_j represent the creation and annihilation operators, respectively; $\boldsymbol{u}_j(\boldsymbol{r})$ represents the wave function of the cavity mode, and ω_j represents the cavity resonant frequency. In the SHG process, energy conservation needs to be satisfied ($2\omega_1 = \omega_2$). Since the cavity modes are orthogonal, the linear part of the Hamiltonian can be expressed as

$$H_{\mathrm{l},j} = \int \boldsymbol{E}_j \cdot \varepsilon_0 \varepsilon_j \boldsymbol{E}_j \,\mathrm{d}V. \tag{1}$$

Here, ε_0 is the vacuum permittivity, and ε_j is the relative permittivity of the medium. Substituting $\boldsymbol{E}_j(r,t)$ into Eq. (1) yields

$$H_{\mathrm{l},j} = \varepsilon_0 \int \varepsilon_j \left|\boldsymbol{u}_j(\boldsymbol{r})\right|^2 \mathrm{d}\boldsymbol{r} \left(2a_j a_j^{\dagger} + 1\right). \tag{2}$$

Since the linear part of the Hamiltonian represents the electric field energy, we can obtain a normalized condition

$$\varepsilon_0 \int \varepsilon_j \left|\boldsymbol{u}_j(\boldsymbol{r})\right|^2 \mathrm{d}\boldsymbol{r} = \frac{\hbar\omega_j}{2}. \tag{3}$$

For the nonlinear part, we consider the second-order term of the Hamiltonian, which is expressed as

$$\begin{aligned} H_{\mathrm{nl}} = {} & \frac{1}{2}\int (\boldsymbol{E}_1(\boldsymbol{r},t) + \boldsymbol{E}_2(\boldsymbol{r},t)) \cdot \varepsilon_0 \chi^{(2)} \\ & : (\boldsymbol{E}_1(\boldsymbol{r},t) + \boldsymbol{E}_2(\boldsymbol{r},t))(\boldsymbol{E}_1(\boldsymbol{r},t) + \boldsymbol{E}_2(\boldsymbol{r},t)). \end{aligned} \tag{4}$$

Here, $\chi^{(2)}$ is the second-order nonlinear optical susceptibility. Substituting $\boldsymbol{E}_j(r,t)$ and according to the conservation of energy, we obtain

$$\begin{aligned} H_{\mathrm{nl}} = {} & \frac{3}{2}\int \boldsymbol{u}_2^{*}(\boldsymbol{r}) \cdot \varepsilon_0 \chi^{(2)} : \boldsymbol{u}_1(\boldsymbol{r})\boldsymbol{u}_1(\boldsymbol{r})\,\mathrm{d}\boldsymbol{r} a_1^2 a_2^{\dagger} \\ & + \frac{3}{2}\int \boldsymbol{u}_2(\boldsymbol{r}) \cdot \varepsilon_0 \chi^{(2)} : \boldsymbol{u}_1^{*}(\boldsymbol{r})\boldsymbol{u}_1^{*}(\boldsymbol{r})\,\mathrm{d}\boldsymbol{r} \left(a_1^{\dagger}\right)^2 a_2. \end{aligned} \tag{5}$$

We introduce the interacting coupling strength g expressed as

$$\hbar g = \frac{3}{2}\int \boldsymbol{u}_2^{*}(\boldsymbol{r}) \cdot \varepsilon_0 \chi^{(2)} : \boldsymbol{u}_1(\boldsymbol{r})\boldsymbol{u}_1(\boldsymbol{r})\mathrm{d}\boldsymbol{r}. \tag{6}$$

Then, Eq. (5) can be rewritten as $H_{\mathrm{nl}} = \hbar\left[g^{*}\left(a_1^{\dagger}\right)^2 a_2 + g a_1^2 a_2^{\dagger}\right]$. The coupling strength represents the interaction of the cavity modes in the SHG process.

The electric field of the cavity modes with rotational symmetry in the microsphere cavity can be expressed as[35] $\boldsymbol{u}_{1(2)}(\boldsymbol{r}) = \boldsymbol{u}_{1(2)}(r,\theta)\,\mathrm{e}^{\mathrm{i}m_{1(2)}\phi}$, where $m_{1(2)}$ is the angular momentum of the pump mode and the SH mode, respectively. $\boldsymbol{P}^{(2)}$ is the second-order nonlinear polarization, which is expressed as[16] $\boldsymbol{P}^{(2)} = \varepsilon_0\chi^{(2)} : \boldsymbol{u}_1(r,\theta)\boldsymbol{u}_1(r,\theta)$. Therefore, Eq. (6) can be rewritten as

$$\hbar g = \frac{3}{2}\int_{\mathrm{WS}_2} \mathrm{e}^{\mathrm{i}(m_2 - 2m_1)\phi}\,\mathrm{d}\phi \int_{\mathrm{WS}_2} \boldsymbol{u}_2^{*}(r,\theta) \cdot \boldsymbol{P}^{(2)} \mathrm{d}r\mathrm{d}\theta. \tag{7}$$

Because of the structural symmetry, the second-order nonlinear optical susceptibilities are $\chi^{(2)}_{\mathrm{WS}_2} = -\chi^{(2)}_{bbb} = -\chi^{(2)}_{baa} = -\chi^{(2)}_{aba} = -\chi^{(2)}_{aab} = 4.5$ nm/V,[11] where a is the zigzag direction and b is the armchair direction of monolayer WS_2. Since WS_2 is on a spherical surface, the stress from bending is uniform, leading to the uniform $\chi^{(2)}$ of monolayer WS_2.[16] The second-order nonlinear polarization components of each direction are

$$\begin{aligned} P_a^{(2)} &= -2\varepsilon_0\chi^{(2)}_{\mathrm{WS}_2} u_a u_b, \\ P_b^{(2)} &= \varepsilon_0\chi^{(2)}_{\mathrm{WS}_2}(-u_a u_a + u_b u_b). \end{aligned} \tag{8}$$

Since monolayer WS_2 is deposited on the surface of the microsphere cavity, we can express $P^{(2)}_{a(b)}$ in the surface coordinates as follows:

$$P^{(2)}_x = \varepsilon_0 \chi^{(2)}_{WS_2}[(u^2_{1,x} - u^2_{1,y})\sin(3\Omega) - 2u_{1,x}u_{1,y}\cos(3\Omega)],$$
$$P^{(2)}_y = \varepsilon_0 \chi^{(2)}_{WS_2}[(u^2_{1,y} - u^2_{1,x})\cos(3\Omega) - 2u_{1,x}u_{1,y}\sin(3\Omega)]. \quad (9)$$

Therefore, the coupling strength can be further obtained by

$$\hbar g = \frac{3}{2}\varepsilon_0 \chi^{(2)}_{WS_2} \int_{WS_2} e^{i(m_2 - 2m_1)\phi} d\phi A_0. \quad (10)$$

Here,

$$A_0 = \int_{WS_2} \{u^*_{2,y}[(u^2_{1,y} - u^2_{1,x})\cos(3\Omega) - 2u_{1,x}u_{1,y}\sin(3\Omega)] + u^*_{2,x}[(u^2_{1,x} - u^2_{1,y})\sin(3\Omega) - 2u_{1,x}u_{1,y}\cos(3\Omega)]\} dr d\theta. \quad (11)$$

For the integral over ϕ, g is nonzero only when $m_2 - 2m_1 = 0$, which corresponds to the momentum-conservation condition.[35] We substitute the energy normalization condition and introduce the effective mode overlap factor as

$$\zeta = \frac{A_0}{\sqrt{\int |u_2(r,\theta)|^2 dr d\theta}(\sqrt{\int |u_1(r,\theta)|^2 dr d\theta})^2}, \quad (12)$$

and the coupling strength is simplified to

$$g \approx \frac{3\chi^{(2)}_{WS_2} l}{16\pi R\sqrt{\pi R}} \zeta \sqrt{\frac{\hbar\omega_2\omega_1^2}{\varepsilon_0\varepsilon_1^2\varepsilon_2}}. \quad (13)$$

Here, we approximate that the radius (R) of the microsphere is much larger than the width of the cavity mode in the radius direction.[35] The coupling strength is proportional to l, which is the size of the material. By normalizing the coupling strength with l, we obtain the coupling strength

$$g \approx \frac{3\chi^{(2)}_{WS_2}}{16\pi R\sqrt{\pi R}} \zeta \sqrt{\frac{\hbar\omega_2\omega_1^2}{\varepsilon_0\varepsilon_1^2\varepsilon_2}}. \quad (14)$$

We choose wavelengths of 1550 nm for the pump mode and 775 nm for the SH mode. For monolayer WS_2, only the electric field in the material plane contributes to the SHG process. Compared with the transverse magnetic (TM) mode, the electric field component of the transverse electric (TE) mode is stronger in the material plane.[36] Therefore, we choose the fundamental TE (TE_0) mode as the pump mode. The SH mode should satisfy both energy conservation ($2\omega_1 = \omega_2$) and momentum conservation ($2m_1 = m_2$) to obtain a large SH signal. Since the mode dispersion is used to compensate for the material dispersion,[35] we need a different mode from the TE_0 mode for the second harmonic. The symmetry of the odd- or even-order SH mode will affect the nonlinear coupling strength with the pump mode, and we discuss these different cases.

For the even-order TE SH mode, the profile of the cavity mode is symmetrical. In this situation, we choose the TE_2 mode as a typical sample. The resonance frequency detuning of the pump mode and SH mode is zero when the condition of momentum is fulfilled ($2m_1 = m_2$) to satisfy the conservation of energy. The detuning of the resonant frequency is denoted as $\delta = (\omega_1 - \omega_2/2)$. We show the relationship between the resonance frequency detuning and the microsphere radius in Fig. 2(a). The blue points in this figure are the simulated frequency detuning, and the red curve is the fitting curve with polynomial fitting. The frequency detuning is zero when the radius is about 112 μm. Although it is difficult to precisely control the radius of the microsphere cavity, the frequency detuning can be tuned to zero by thermal and Kerr effects[36] to achieve ideal conditions in the experiment. To show the symmetry of the electric field, the y component of the electric field (E_y) profiles of the pump mode and the SH mode are shown in Figs. 2(b) and 2(c), respectively. The E_y of the pump mode has the same sign. Different from the pump mode, the E_y of the SH mode can be positive or negative in different positions, which may lead to the cancelation of the coupling strength. Therefore, we investigate the effect of material position on the coupling strength. The dependence of the coupling strength g on the material position θ is shown in Fig. 2(d), where w is 5 μm and Ω is 0°. Three peaks of coupling strength can be found, and the strongest coupling strength occurs at $\theta = 0°$ due to the symmetry of the SH (TE_2) mode. We further scan w of the material to find the dependence of the coupling strength on the range of the interaction area at $\theta = 0°$, as shown in Fig. 2(e). We obtain a maximum coupling strength of 1556 Hz/μm when w is 4.2 μm. As the material coverage continuously increases, the coupling strength decreases because of the cancelation.

For the odd-order TE SH mode, the profile of the cavity mode is anti-symmetry. In general, SHG conversion will be canceled by the anti-symmetric mode profile.[35] However, the flexible choice of position and size of monolayer WS_2 can avoid cancelation caused by the anti-symmetric mode profile. To study this case, we choose the TE_3 mode as a typical sample. The frequency detuning dependence on the microsphere radius is illustrated in Fig. 3(a). The frequency detuning is zero when the radius is around 88 μm. The E_y profile of the SH mode is shown in Fig. 3(c), which exhibits anti-symmetry different from the TE_2 mode. The dependence of the coupling strength on the position (θ) of the material is shown in Fig. 3(d), where w is 5 μm and Ω is 0°. Due to the anti-symmetry of the TE_3 mode, the coupling strength is minimal when θ is 0°. We find that the coupling strength reaches a maximum when θ is 1.2°. In this position, the dependence of the coupling strength on w of the material is shown in Fig. 3(e). We obtain the maximum coupling strength of 2225 Hz/μm when w is 3.9 μm.

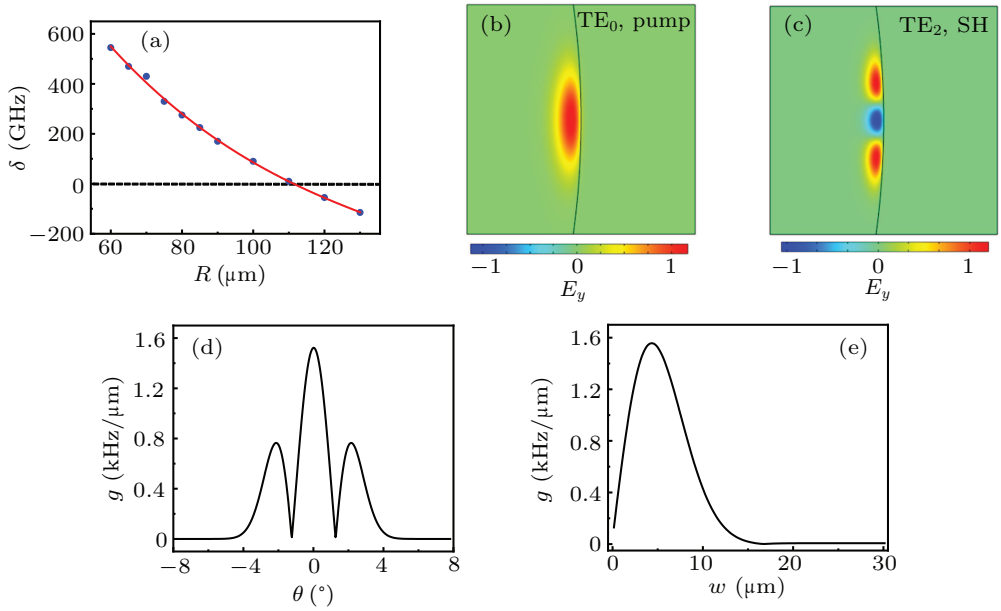


Fig. 2. (a) The resonance frequency detuning $[\delta = (\omega_1 - \omega_2/2)]$ of pump mode (TE_0, ω_1) and SH mode (TE_2, ω_2) depending on the microsphere radius. Here, the black dashed line is $\delta = 0$. (b) Normalized y component of the electric field (E_y) profile of pump mode (TE_0). (c) Normalized E_y profile of the SH mode (TE_2). (d) Dependence of the coupling strength between the TE_0 mode and TE_2 mode on the position of the material. (e) Dependence of the coupling strength between the TE_0 mode and TE_2 mode on w of the material.

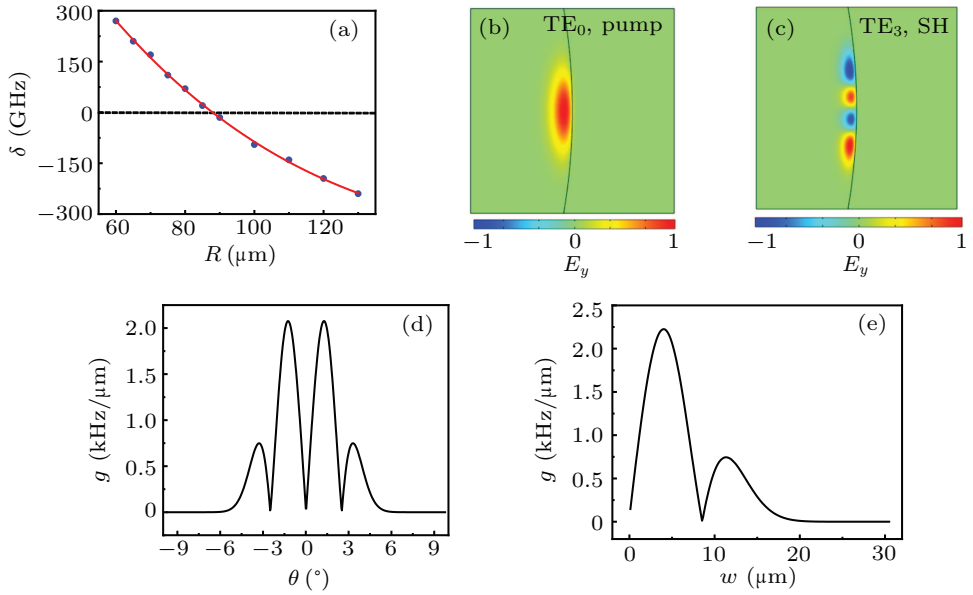


Fig. 3. (a) The resonance frequency detuning $[\delta = (\omega_1 - \omega_2/2)]$ of pump mode (TE_0, ω_1) and SH mode (TE_3, ω_2) depending on the microsphere radius. Here, the black dashed line is $\delta = 0$. (b) Normalized E_y profile of pump mode (TE_0). (c) Normalized E_y profile of the SH mode (TE_3). (d) Dependence of the coupling strength between the TE_0 mode and TE_3 mode on the position of the material. (e) Dependence of the coupling strength between the TE_0 mode and TE_3 mode on w of the material.

Furthermore, we analyze the coupling strength when the SH mode is the fundamental TM (TM_0) mode. The frequency detuning dependence on the microsphere radius is illustrated in Fig. 4(a). The frequency detuning is zero when the radius is around 140 μm. The pump mode and the SH mode have different electric field polarizations on the surface of the microsphere, as shown in Figs. 4(b) and 4(c), respectively. E_x is much stronger than E_y of the TM_0 mode (SH) in the plane of the material.[36] We can generate SHG with E_x by rotating the crystal orientation of the material. The E_x profiles of the pump mode and the SH mode are shown in Fig. 4(d). The dependence of the coupling strength on the position (θ) of the material is shown in Fig. 4(d), where w is 5 μm. Ω is 90° to ensure that the coupling strength is affected by E_x with Eq. (9). The coupling strength reaches a maximum when θ is 0° because of mode symmetry. We further find that the coupling strength increases with the range of the interaction area as shown in Fig. 3(e), because the E_x of the TM_0 mode has the same sign on the microsphere surface. The coupling strength is 1250 Hz/μm when the material completely covers the range of the cavity mode on the microsphere surface.

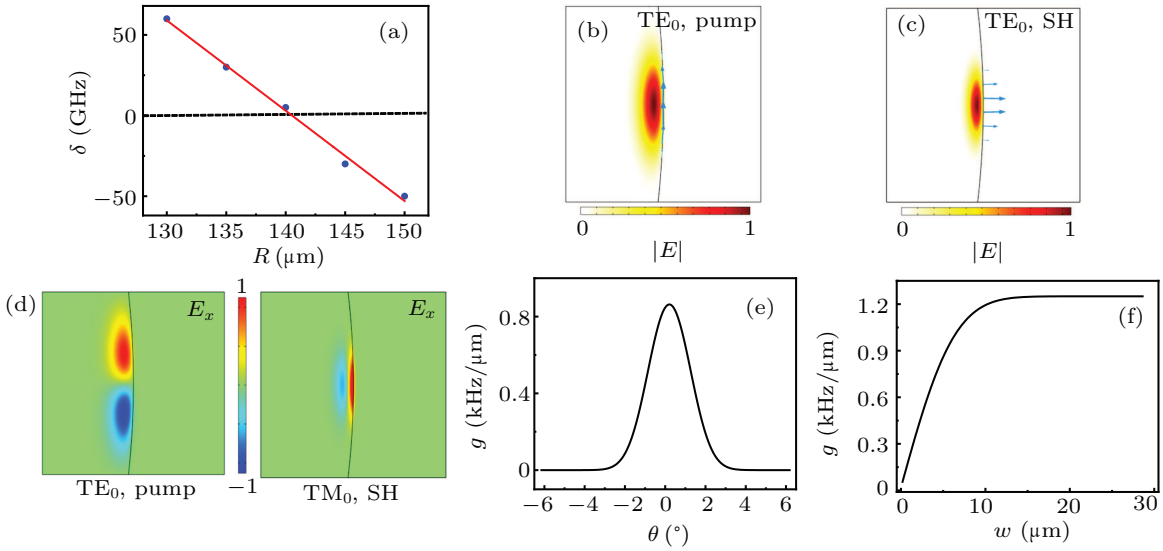


Fig. 4. (a) The resonance frequency detuning $[\delta = (\omega_1 - \omega_2/2)]$ of pump mode (TE_0, ω_1) and SH mode (TM_0, ω_2) depending on the microsphere radius. Here, the black dashed line is $\delta = 0$. (b) Normalized electric field intensity ($|E|$) profile of pump mode (TE_0). The blue arrows represent the direction of electric field polarization. (c) Normalized $|E|$ profile of the SH mode (TM_0). The blue arrows represent the direction of electric field polarization. (d) Normalized electric field component in x-direction (E_x) profiles of the pump and SH modes. (e) Dependence of the coupling strength between the TE_0 mode and TM_0 mode on the position of the material. (f) Dependence of the coupling strength between the TE_0 mode and TM_0 mode on w of the material.

According to the results, we obtain the strongest coupling strength, which is $g = 2225$ Hz/μm. Here, the pump mode is the TE_0 mode, the SH mode is the TE_3 mode, θ is 1.2°, and w is 3.9 μm. We further study the influence of crystal orientation on the coupling strength with these parameters. The dependence of the coupling strength on Ω is shown in Fig. 5(a). This dependence is similar to the polarization dependence of the SHG generated by the free-space linearly polarized pump laser because of the structural symmetry of monolayer WS_2.[11] The total Hamiltonian of the SHG process can be expressed as[35]

$$H = \omega_1 a_1^\dagger a_1 + \omega_2 a_2^\dagger a_2 + \hbar\left[g^*\left(a_1^\dagger\right)^2 a_2 + g a_1^2 a_2^\dagger\right] + \varepsilon_p(a_1 e^{i\omega_1 t} + a_1^\dagger e^{-i\omega_1 t}),$$

where ε_p is the input pump strength. Considering the SHG process with low pump power and low conversion efficiency, the relative SHG conversion efficiency can be expressed as[35]

$$\eta = \frac{P_{SHG}}{P_{pump}^2} = \frac{16 g^2 l^2}{\left(\frac{\kappa_{2,0}}{\sqrt{\kappa_{2,1}}} + \sqrt{\kappa_{2,1}}\right)^2 \left(\frac{\kappa_{1,0}}{\sqrt{\kappa_{1,1}}} + \sqrt{\kappa_{1,1}}\right)^4} \frac{1}{\hbar\omega_1}, \quad (15)$$

where $\kappa_{1(2),0}$ are the intrinsic loss rates and $\kappa_{1(2),1}$ are the intrinsic loss rates of the pump mode and SH mode, respectively. Here, the loss rate is expressed as $\kappa = \frac{\omega}{2Q}$, with Q being the quality factor corresponding to the loss. To calculate the SHG conversion efficiency, we choose typical intrinsic quality factors ($Q_{1(2),0}$) as 1×10^6. The absolute power conversion efficiency (P_{SHG}/P_{pump}) against the external coupling quality factor is shown in Fig. 5(b), where l is 1 μm and the pump power is 1 mW. The conversion efficiency requires a critical coupling condition for both modes to reach the maximum value of approximately 3.35% and the maximum relative conversion efficiency of $\eta = P_{SHG}/P_{pump}^2 \approx 3350\ \% \cdot W^{-1}$. This result is much higher than the conversion efficiency reported in the existing work, where the conversion efficiency is about 0.002% with a pump power of 2 mW.[33]

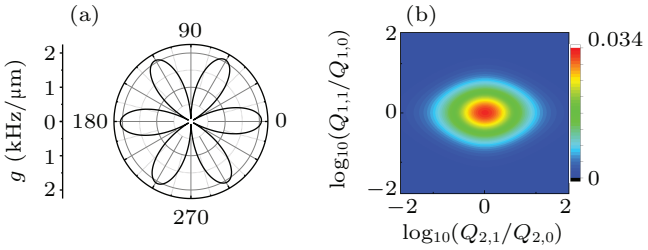


Fig. 5. (a) Dependence of the coupling strength on Ω. Here the pump mode is the TE_0 mode, the SH mode is the TE_3 mode, θ is 1.2°, and w is 3.9 μm. (b) Absolute power conversion efficiency (P_{SHG}/P_{pump}) against the external coupling quality factor ($Q_{1(2),1}$). In the calculation, the intrinsic quality factors ($Q_{1(2),0}$) are 1×10^6, and the pump power is 1 mW.

4. Conclusion

In summary, we have theoretically studied the SHG of monolayer WS_2 coupled with a silica microsphere cavity. We consider that monolayer WS_2 is deposited on a microsphere with different positions, sizes, and crystal orientations and flexibly matches different modes with odd/even order or different polarization directions. We calculate the dependence of the coupling strength in these cases. The theoretical calculation of the optimal SHG conversion efficiency is 3.35% under the typical quality factor (1×10^6) and pump power (1 mW). Increasing the length of the material in the x-direction, im-

proving the quality factor of the cavity, and increasing the pump power can further increase the SHG conversion efficiency. These results provide guidance to achieve optimal second-order nonlinear response with the microsphere cavity-coupled two-dimensional material, which will be further used in more applications for integrated optical systems.

Acknowledgements

Project supported by the National Natural Science Foundation of China (Grant Nos. 11774333 and 62061160487) and the Fundamental Research Funds for the Central Universities.

References

[1] Yu S, Wu X, Wang Y, Guo X and Tong L 2017 *Adv. Mater.* **29** 1606128
[2] Gutiérrez H R, Perea-López N, Elías A L, Berkdemir A, Wang B, Lv R, López-Urías F, Crespi V H, Terrones H and Terrones M 2013 *Nano Lett.* **13** 3447
[3] Liu D, Yu L, Xiong X, Yang L, Li Y, Li M, Li H O, Cao G, Xiao M, Xiang B, Min C, Guo G C, Ren X F and Guo G P 2016 *Opt. Express* **24** 27554
[4] Yu L, Liu D, Qi X Z, Xiong X, Feng L T, Li M, Guo G P, Guo G C and Ren X F 2018 *Chin. Phys. B* **27** 047302
[5] Zhao W, Ghorannevis Z, Chu L, Toh M, Kloc C, Tan P H and Eda G 2013 *ACS Nano* **7** 791
[6] Zhou L, Fu H, Lv T, Wang C, Gao H, Li D, Deng L and Xiong W 2020 *Nanomaterials* **10** 2263
[7] Autere A, Jussila H, Dai Y, Wang Y, Lipsanen H and Sun Z 2018 *Adv. Mater.* **30** 1705963
[8] Ribeiro-Soares J, Janisch C, Liu Z, Elías A L, Dresselhaus M S, Terrones M, Cançado L G and Jorio A 2015 *2D Mater.* **2** 045015
[9] Zhao M, Ye Z, Suzuki R, Ye Y, Zhu H, Xiao J, Wang Y, Iwasa Y and Zhang X 2016 *Light Sci. Appl.* **5** e16131
[10] Jiang H, Zheng L, Wang J, Xu M, Gan X, Wang X and Hang W 2021 *Nanoscale* **13** 18103
[11] Janisch C, Wang Y, Ma D, Metha N, Elías A L, Perea-López N, Terrones M, Crespi V and Liu Z 2014 *Sci. Rep.* **4** 5530
[12] Liu N, Yang X, Zhu Z, Chen F, Zhou Y, Xu J and Liu K 2022 *Nanoscale* **14** 49
[13] Chen H, Corboliou V, Solntsev A S, Choi D Y, Vincenti M A, Ceglia D, Angelis C, Lu Y and Neshev D N 2017 *Light Sci. Appl.* **6** e17060
[14] Zuo Y, Yu W, Liu C, Chen X, Qiao R, Liang J, Zhou X, Wang J, Wu M, Zhao Y, Gao P, Wu S, Sun Z, Liu K, Bai X and Liu Z 2020 *Nature Nanotech.* **15** 987
[15] Li W, Chen B, Meng C, Fang W, Xiao Y, Li X, Hu Z, Xu Y, Tong L, Wang H, Liu W, Bao J and Shen Y R 2014 *Nano Lett.* **14** 955
[16] Chen J, Tan J, Wu G, Zhang X, Xu F and Lu Y 2019 *Light Sci. Appl.* **8** 1
[17] Tan T, Yuan Z, Zhang H, Yan G, Zhou S, An N, Peng B, Soavi G, Rao Y and Yao B 2021 *Nat. Commun.* **12** 6716
[18] Li X, Liu W, Song Y, Zhang C, Long H, Wang K, Wang B and Lu P 2019 *Adv. Opt. Mater.* **7** 1801270
[19] Liu D, Qi X Z, Chiu K L, Taniguchi T, Ren X F and Guo G P 2018 *Chin. Phys. B* **27** 087303
[20] Ye Y, Wong Z J, Lu X, Ni X, Zhu H, Chen X, Wang Y and Zhang X 2015 *Nat. Photon.* **9** 733
[21] Qi X, Lo T W, Liu D, Feng L, Chen Y, Wu Y, Ren H, Guo G C, Lei D Y and Ren X F 2020 *Nanophotonics* **9** 2097
[22] Sun L, Hu H, Zhan D, Yan J, Liu L, Teguh J S, Yeow E K L, Lee P S and Shen Z 2014 *Small* **10** 1090
[23] Akselrod G M, Ming T, Argyropoulos C, Hoang T B, Lin Y, Ling Xi, Smith D R, Kong J and Mikkelsen M H 2015 *Nano Lett.* **15** 3578
[24] Zheng D, Zhang S, Deng Q, Kang M, Nordlander P and Xu H 2017 *Nano Lett.* **17** 3809
[25] Wu Y, Liu X, Qi X, Lu L, Guo G, Guo G C and Ren X F 2021 *Appl. Phys. Lett.* **118** 104002
[26] Liu C P, Zhu X L, Zhang J S, Xu J, Wang Y M and Yu D P 2016 *Chin. Phys. B* **33** 087303
[27] Wang H, Wen J, Wang W, Xu N, Liu P, Yan J, Chen H and Deng S 2019 *ACS Nano* **13** 1739
[28] Wu S, Buckley S, Schaibley J R, Feng L, Yan J, Mandrus D G, Hatami F, Yao W, Vučković J, Majumdar A and Xu X 2015 *Nature* **520** 69
[29] Zhang L, Gogna R, Burg W, Tutuc E and Deng H 2018 *Nat. Commun.* **9** 713
[30] Hu G, Hong X, Wang K, Wu J, Xu H X, Zhao W, Liu W, Shuang Z, Garcia-Vidal, Wang B, Lu P and Qiu C W 2019 *Nat. Photon.* **13** 467
[31] Chen J, Wang K, Long H, Han X, Hu H, Liu W, Wang B and Lu P 2018 *Nano Lett.* **18** 1344
[32] Liu Z, Wang J, Chen B, Wei Y, Liu W and Liu J 2021 *Nano Lett.* **21** 7405
[33] Shi J, Liang W Y, Raja S S, Sang Y, Zhang X Q, Chen C A, Wang Y, Yang X, Lee Y H, Ahn H and Gwo S 2018 *Laser Photon. Rev.* **12** 1800188
[34] Shen Z, Zhang Y L, Chen Y, Zou C L, Xiao Y F, Zou X B, Sun F W, Guo G C and Dong C H 2016 *Nat. Photon.* **10** 657
[35] Guo X, Zou C L and Tang H X 2016 *Optica* **3** 1126
[36] Zhang X, Cao Q T, Wang Z, Liu Y, Qiu C W, Yang L, Gong Q and Xiao Y F 2019 *Nat. Photon.* **13** 21